

Article

# Improving the Performances of Random Copolymer Based Organic Solar Cells by Adjusting the Film Features of Active Layers Using Mixed Solvents

Xiangwei Zhu <sup>1,†</sup>, Kun Lu <sup>1,†</sup>, Benzheng Xia <sup>1</sup>, Jin Fang <sup>1</sup>, Yifan Zhao <sup>1</sup>, Tianyi Zhao <sup>2,\*</sup>, Zhixiang Wei <sup>1,\*</sup> and Lei Jiang <sup>2,\*</sup>

Received: 23 November 2015; Accepted: 24 December 2015; Published: 29 December 2015

Academic Editor: Scott M. Husson

<sup>1</sup> National Center for Nanoscience and Technology, Beijing 100190, China; zhuxw@nanoctr.cn (X.Z.); lvk@nanoctr.cn (K.L.); xiabz@nanoctr.cn (B.X.); fangj@nanoctr.cn (J.F.); zhaoyifan@nanoctr.cn (Y.Z.)

<sup>2</sup> Key Laboratory of Bio-Inspired Smart Interfacial Science and Technology of Ministry of Education, School of Chemistry and Environment, Beihang University, Beijing 100191, China

\* Correspondence: zhaoty@buaa.edu.cn (T.Z.); weizx@nanoctr.cn (Z.W.); jianglei@iccas.ac.cn (L.J.); Tel.: +86-10-8254-5565 (Z.W.); +86-10-8262-1396 (L.J.); Fax: +86-10-6265-6765 (Z.W.); +86-10-8262-7566 (L.J.)

† These authors contributed equally to this work.

**Abstract:** A novel random copolymer based on donor–acceptor type polymers containing benzodithiophene and dithienosilole as donors and benzothiazole and diketopyrrolopyrrole as acceptors was designed and synthesized by Stille copolymerization, and their optical, electrochemical, charge transport, and photovoltaic properties were investigated. This copolymer with high molecular weight exhibited broad and strong absorption covering the spectra range from 500 to 800 nm with absorption maxima at around 750 nm, which would be very conducive to obtaining large short-circuits current densities. Unlike the general approach using single solvent to prepare the active layer film, mixed solvents were introduced to change the film feature and improve the morphology of the active layer, which lead to a significant improvement of the power conversion efficiency. These results indicate that constructing random copolymer with multiple donor and acceptor monomers and choosing proper mixed solvents to change the characteristics of the film is a very promising way for manufacturing organic solar cells with large current density and high power conversion efficiency.

**Keywords:** random copolymer; photovoltaic; mixed solvents; film feature

## 1. Introduction

A mixed bulk heterojunction (BHJ) structure, which consists of a conjugated polymer as an electron donor and a fullerene derivative as an electron acceptor, produces high power conversion efficiency (PCE) in polymer solar cells (PSCs) [1]. Alternating electron donor (D) and acceptor (A) building blocks to construct D–A type polymers is an effective strategy for designing high efficient photovoltaic materials for PSCs [2–4]. The properties of D–A copolymers can be fine-tuned by varying the type of electron-donating or withdrawing unit, respectively. In this way, some highly efficient D–A polymers with improved absorption spectra and proper energy levels have emerged in recent years [5,6].

Current D–A copolymer design strategies include: (1) synthesizing novel donor [7] and acceptor units [8]; (2) introducing  $\pi$ -spacers to construct D- $\pi$ -A polymers [9]; (3) optimizing the alkyl side chains to balance the crystallinity and solubility [10]; and (4) introducing substituents, for example fluorine atoms, to tune the energy levels [11]. In addition to these methods, introducing many different units into the polymer backbone to construct the copolymer is also a promising approach, since

they can exhibit the synergetic effects of each unit by tuning the composition ratio, thus exhibiting red-shifted absorption spectra, proper highest occupied molecular orbital (HOMO) energy levels, higher hole mobility, and greatly improved photovoltaic properties [12]. Such a design strategy creates an intriguing possibility to modify the existing D–A type photovoltaic polymers for better performances. Thus far, there are plenty of examples of significant improvement being achieved by randomly copolymerizing one donor and one acceptor with a third monomer [13–16].

In addition, other strategies have also been carried out to improve the photovoltaic performances of PSCs by tuning the morphologies of the blend films, such as the selecting different preparation solvent, introducing high boil point additive, using mixed solvents and annealing the active layer [17]. Among them, using mixed solvents is a very maneuverable and efficient way [18]. Since different active layer films prepared by diverse solvents have, respectively, special surface energy, reflecting the surface composition of blend film. Furthermore, the performance of BHJ solar cell in part depends on whether polymer or [6,6]-phenyl-C71-butyric acid methyl ester (PC<sub>71</sub>BM) would be enriched on the top surface of the blend film [19]. Besides, mixed solvents can also be effectively used to tune the miscibility of the donor and acceptor components, the domain size and the morphology of active layer, which play an important role in optimizing the photovoltaic performances for PSCs [20–22].

In this study, we adopt an alternative approach for designing copolymer by “doping” a D–A fraction to another D–A copolymer by chemical synthesis. We present a new fully conjugated random copolymer, PSTDPP (see Scheme 1), containing two donor units, silolethiophene (SDT) [23] and benzodithiophene (BDT) [24], and two acceptors, benzothiadiazole (BT) [25] and diketopyrrolopyrrole (DPP) [26]. All of these units are frequently used building blocks for high efficient PSCs [27–30]. The copolymer was synthesized from them via Palladium-catalyzed Stille coupling reaction. The polymer synthesis concerns the copolymerization of three components, in which BDT acts as a bridge, linking the D–A fraction (BT-SDT-BT) and DPP units. As expected, the random polymer exhibits a broad absorption with a range of 500–800 nm and a proper HOMO energy level, which ensure its applicability for fabrication of PSC devices. The best PCE value of 4.38% was obtained by using mixed solvent of *O*-dichlorobenzene (ODCB) and chloroform (CF) with 1,8-octanedithiol (DIO) as additive, which is much better than those of devices using single CF or ODCB as processing solvent. The result suggests that using mixed solvent to prepare the active layer could improve the film characteristic effectively, leading to an enhanced PCE for PSCs.

## 2. Experimental Section

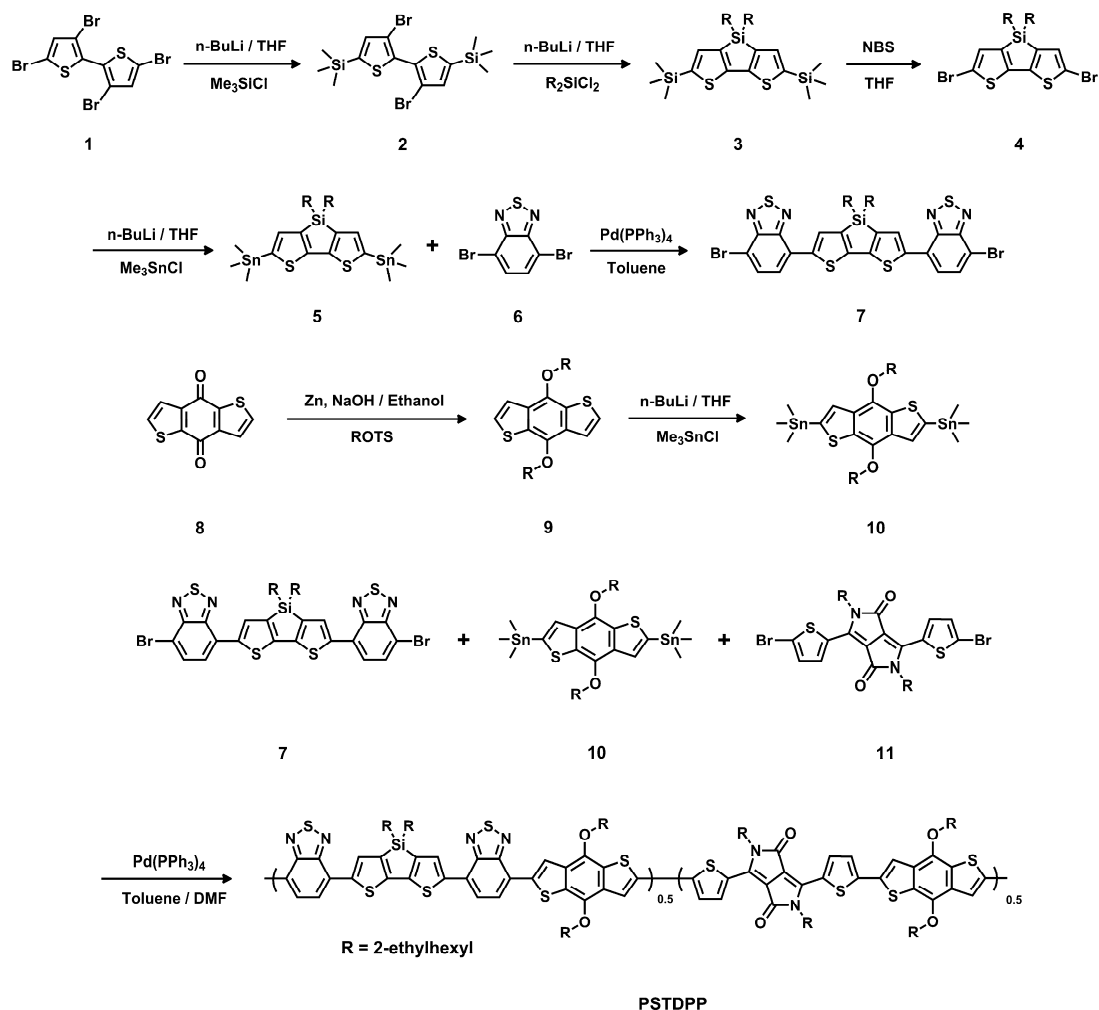
### 2.1. Materials and Synthesis

Solvents and other common reagents were obtained from Beijing Chemical Plant (Beijing, China). All other chemicals were purchased from commercial sources (Alfa Aesar (Heysham, UK), Acros (Geel, Belgium) and Sigma-Aldrich (Saint Louis, MO, USA)) and were used without further purification unless otherwise stated. Tetrahydrofuran, toluene, and chloroform were freshly distilled from appropriate drying agents prior to use. Compounds **1**, **2** [23], **8** [31], **10** [32] and **11** [33] were prepared according to the published literature. The detailed synthetic processes are illustrated in Scheme 1.

### Compound 3

Compound **2** and 40 mL THF were put into a flask, and cooled down to  $-78\text{ }^{\circ}\text{C}$  by a liquid nitrogen–acetone bath. Then, 3.9 mL butyllithium solution in hexane ( $2.7\text{ mol}\cdot\text{L}^{-1}$ ) was added dropwise for 5 min, and the reactant was stirred for another 15 min at that temperature. Subsequently, 1.95 g dichlorodi(2-ethyl-hexyl)silane (6 mmol) was added in one portion, and the cooling bath was removed and the reactant was stirred for 2 h under ambient temperature. Then, the reactant was poured into water and extracted by ethyl ether several times. After removal of volatiles, the residue was purified by silica gel chromatography using hexane as eluent and gave 2.26 g of compound **3** (yield 72%). The product was obtained as colorless oil. GC–MS:  $m/z = 562.2$ .  $^1\text{H}$  NMR ( $\text{CDCl}_3$ ,

400 MHz),  $\delta$  (ppm): 7.06 (s, 2H), 1.71 (m, 2H), 1.51–1.14 (m, 16H), 0.91 (t, 6H), 0.85 (t, 6H), 0.76 (m, 4H), 0.31 (s, 18H).



**Scheme 1.** Synthesis route of the polymer.

#### Compound 4

Compound 3 (1.69 g, 3 mmol) was dissolved into 20 mL THF, and *N*-bromosuccinimide (1.1 g, 6.17 mmol) was added in one portion. The reactant was stirred at ambient temperature for 4 h, and then extracted by diethyl ether. The volatiles were removed under vacuum, and the residue was purified by silica gel chromatography using hexane as eluent. The product was obtained as sticky colorless or pale yellow oil with a yield of 96%. MS (MALDI-TOF):  $m/z = 576.0$ .  $^1\text{H NMR}$  ( $\text{CDCl}_3$ , 400 MHz),  $\delta$  (ppm): 6.97 (s, 2H), 1.72 (m, 2H), 1.51–1.13 (m, 16H), 0.91 (t, 6H), 0.83 (t, 6H), 0.76 (m, 4H).

#### Compound 5

Compound 4 (1.2 g, 2.51 mmol) and 20 mL ultra-dry THF were put into a flask. The clear solution was cooled down to  $-78^\circ\text{C}$  by a liquid nitrogen–acetone bath. Then, 2.4 mL butyllithium solution in hexane (2.3 mmol, 2.4 mol/L) was added dropwise. After stirring at  $-78^\circ\text{C}$  for 15 min, 7 mL trimethyltin chloride (1 mol/L) was added in one portion, and then the cooling bath was removed. After being stirred at ambient temperature for 2 h, the reactant was poured into cool water and extracted by diethyl ether several times. After removal of volatiles, the product (1.78 g, 2.39 mmol) was obtained as sticky pale green oil with a yield of 95% and used without any further purification. MS

(MALDI-TOF):  $m/z = 744.1$ .  $^1\text{H NMR}$  ( $\text{CDCl}_3$ , 400 MHz),  $\delta$  (ppm): 7.03 (s, 2H), 1.68 (m, 2H), 1.4–1.13 (m, 16H), 0.90 (t, 6H), 0.83 (t, 6H), 0.74 (m, 4H).

#### Compound 7 [34]

Compound 5 (760 mg, 1.02 mmol), compound 6 (1.8 g, 6.11 mmol),  $\text{Pd}(\text{PPh}_3)_4$  (0.100 g, 0.08 mmol), and toluene (15 mL) were put into a 50 mL flask and stirred under  $\text{N}_2$  protection for 20 min. The mixture was heated to 80 °C for 10 min, 100 °C for 10 min and 150 °C for 5 h. Upon cooling, the red residue was passed through a short silica plug eluting with  $\text{CHCl}_3$  (500 mL). All volatiles were removed *in vacuo* to give the crude product as a dark sticky solid. The material was then slurried in methanol (300 mL), filtered, loaded onto silica using  $\text{CHCl}_3$  and purified by flash chromatography using a hexanes/ $\text{CHCl}_3$  gradient. The product eluted as a red solution at 40%  $\text{CHCl}_3$ . After fraction collection and solvent removal, the solid product was slurried in methanol (300 mL), sonicated for 30 min, and filtered. The solid was washed with copious amounts of methanol and acetone, and then dried under vacuum for 24 h. The product was collected as green/purple metallic colored powder. Yield = 45%. MS (MALDI-TOF):  $m/z = 844.0$ .  $^1\text{H NMR}$  ( $\text{CDCl}_3$ , 400 MHz),  $\delta$  (ppm): 8.17 (m, 2H), 7.82 (d, 2H), 7.68 (d, 2H), 1.54 (m, 2H), 1.33 (m, 4H), 1.28 (m, 4H), 1.21 (m, 8H), 1.10 (m, 4H), 0.82 (m, 12H).

#### PSTDPP

Compound 7 (0.42 g, 0.5 mmol), compound 10 (0.77 g, 1 mmol) and compound 11 (0.34 g, 0.5 mmol) were dissolved into anhydrous toluene (10 mL) in a three-neck flask. The solution was flushed with argon for 20 min, and then  $\text{Pd}(\text{PPh}_3)_4$  (50 mg, 0.043 mmol) was added into the flask. The flask was subjected to three successive cycle of vacuum followed by refilling with argon. Then, the polymerization was carried out at 110 °C for 18 h under argon protection. After cooling to room temperature, the reaction mixture was dripped into 100 mL of methanol with vigorous stirring. The polymer precipitate was collected by filtration and transferred to a thimble. After drying, the crude polymer was subjected to Soxhlet extraction using methanol, acetone, hexane and chloroform as solvents. After final extraction with chloroform, the chloroform solution was concentrated to approximately 10 mL and then dripped into 100 mL of methanol with vigorous stirring. The polymer was collected by filtration and dried to afford a solid as the product. Yield = 72%,  $M_n = 21.6$  kDa and PDI = 3.47.

#### 2.2. Measurements

Mass Spectra were determined on Bruker microflex MALDI-TOF mass spectrometer (Bruker, Billerica, MA, USA).  $^1\text{H NMR}$  (400 MHz) was obtained on a Bruker avance 400 NMR Spectrometer (Bruker, Billerica, MA, USA) using tetramethylsilane as internal standard. UV–Vis absorption spectra were recorded on a Shimadzu UV-3600 UV–vis–NIR spectrophotometer (Shimadzu, Kyoto, Japan). The electrochemical cyclic voltammetry (CV) was conducted on an EG&G Princeton Applied Research VMP3 workstation (Bio-Logic, Claix, France) with Pt disk coated with the polymer film, Pt plate, and  $\text{Ag}/\text{Ag}^+$  electrode as working electrode, counter electrode and reference electrode respectively in a  $0.1 \text{ mol}\cdot\text{L}^{-1}$  tetrabutylammoniumhexafluorophosphate ( $\text{Bu}_4\text{NPF}_6$ ) acetonitrile solution. The current density–voltage ( $J$ – $V$ ) curves were obtained by a Keithley 2420 source-measure unit (Keithley, Cleveland, OH, USA). The photocurrent was measured under illumination using an Oriol Newport 150W solar simulator (AM 1.5G, Newport, Irvine, CA, USA), and the light intensity was calibrated with a Newport reference detector (Oriol PN 91150V, Newport, Irvine, CA, USA). The external quantum efficiency (EQE) measurements of the devices were performed in air with an Oriol Newport system (Model 66902, Newport, Irvine, CA, USA). The thickness of the active layer was measured on a Kla-TencorAlpha-StepD-120 Stylus Profiler (Kla-TencorAlpha-StepD-120 Stylus Profiler). X-ray diffraction (XRD) measurements were carried out in the reflection mode at room temperature using a 12-Kw D/max-rA X-ray diffraction system (12-kW D/max-rA X-ray diffraction system). The step size for all scans was 4 degree with a count time of 1 min per step. Atomic Force

Microscope (AFM) images were obtained on a NanoscopeIIIa AFM Multimode Digital Instrument (Bruker, Billerica, MA, USA) in tapping mode.

### 2.3. Organic Field-Effect Transistor (OFET) Devices Fabrication and Measurement

OFETs were constructed on octadecyltrichlorosilane (OTS) modified SiO<sub>2</sub>/Si substrates with top-contact configuration. The 10 mg·mL<sup>-1</sup> ODCB solutions of the polymers were spin-coated on the substrates in air at room temperature. The source and drain electrodes were patterned through the mask using thermal evaporation method. The channel length were 100 μm and the ratio of channel width to channel length  $W/L = 110$ . The mobility in the saturation regime was determined using the equation:  $I_{DS} = (\mu_{FET} \cdot W \cdot C_i / 2L)(V_G - V_T)^2$ , where  $I_{DS}$  is the drain-source current in the saturated regime,  $\mu_{FET}$  is the field-effect mobility,  $W$  the channel width,  $L$  the channel length,  $C_i$  the capacitance SiO<sub>2</sub> dielectric layer,  $V_G$  the gate voltage and  $V_T$  the threshold voltage.

### 2.4. PSC Devices Fabrication and Measurement

Polymer solar cell devices with the structure glass/indium tin oxide (ITO)/poly(3,4-ethylenedioxythiophene):poly(styrenesulfonate) (PEDOT:PSS)/polymer:PC<sub>71</sub>BM( $w/w$ )/Ca/Al were fabricated as follows: The PEDOT:PSS solution was spin-coated on top of the cleaned ITO-coated glass substrate and the film thickness was approximately 40 nm. Then the coated substrates were transferred into a glove box. The polymer/PC<sub>71</sub>BM blend solution used in this study for spin-coating was 10 mg·mL<sup>-1</sup> for the different solutions. The additive, DIO, was added prior to spin-coating process. The thickness of the active layer was controlled by changing the spin speed during the spin-coating process and distributed around 100 nm. The devices were completed by evaporating Ca/Al metal electrodes with an area of 4 mm<sup>2</sup> as defined by masks. These layers were thermally evaporated at a pressure of  $2 \times 10^{-6}$  Torr. To optimize device performance, different D/A weight ratios ( $w/w$ ) and different solution were used during the device fabrication process.

## 3. Results and Discussion

### 3.1. Optical and Electrochemical Properties

The optical property of PSTDPP was investigated by UV–vis absorption spectra both in chloroform solution and thin films. As shown in Figure 1, the polymer showed a relatively broad absorption in the UV–vis range. The absorption spectrum of PSTDPP in chloroform solution and at solid state showed absorption maximum at 677/738 and 683/747 nm, respectively. Compared with the absorption in solution, a very slight red shift of the spectrum for the solid state was observed. The optical band gap of PSTDPP can be calculated from the film absorption edge as 1.53 eV.

The electrochemical property of the polymer was investigated by cyclic voltammetry (CV) method. As shown in Figure 2, the polymer showed reversible *p*-doping/dedoping (oxidation/re-reduction) and *n*-doping/dedoping (reduction/reoxidation) processes. The energy levels of the highest occupied molecular orbital (HOMO) and the lowest unoccupied molecular orbital (LUMO) can be calculated from the onset oxidation and reduction potentials according to the equation: HOMO =  $-e(E^{\text{ox}} + 4.71)$  (eV) and LUMO =  $-e(E^{\text{red}} + 4.71)$  (eV) [35]. The electrochemical band gaps ( $E_g^{\text{ec}}$ ) can be calculated from the equation:  $E_g^{\text{ec}} = (E^{\text{ox}} - E^{\text{red}})$  (eV). The HOMO levels and the LUMO levels of PSTDPP were estimated to be at  $-5.15$  eV and  $-3.47$  eV, respectively. The corresponding electrochemical band gap of PSTDPP was 1.68 eV.

### 3.2. Crystallinity

To gain a deeper insight of the crystallinity and molecular stacking mode of the polymer, X-ray diffraction (XRD) analysis of the polymer film spin-coated on the quartz substrate was operated (Figure 3). The PSTDPP film shows a distinct diffraction peak (100) at  $2\theta$  around  $4.2^\circ$ , indicating the chains form a interdigitation packing structure in the film with interchain *d*-spacing distance of 21.0 Å.

The peak around  $20^{\circ}$ – $25^{\circ}$  for the polymer can be assigned to the face-to-face stacking of the aromatic groups arranged in the parallel direction [36]. The polymer exhibited good crystallinity and formed highly ordered structure in the film, which was expected to afford high hole mobility and facilitate charge carrier transport in BHJ solar cells.

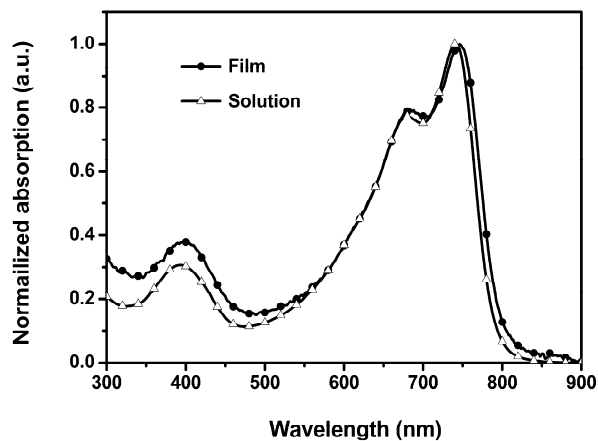


**Figure 1.** UV-vis absorption spectra of PSTDPP in  $1 \times 10^{-5}$  M chloroform solution and at solid state.

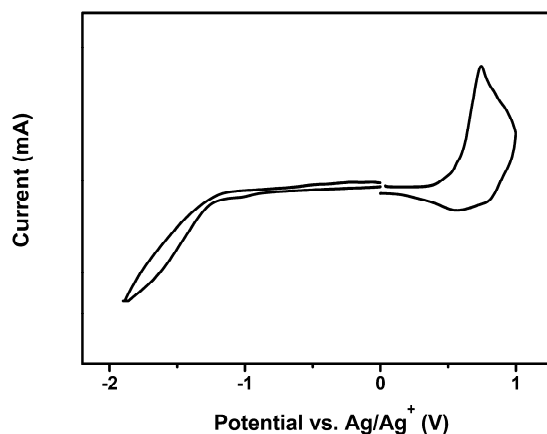


**Figure 2.** Cyclic voltammetry (CV) curves of PSTDPP at a scan speed of  $50 \text{ mV s}^{-1}$ .

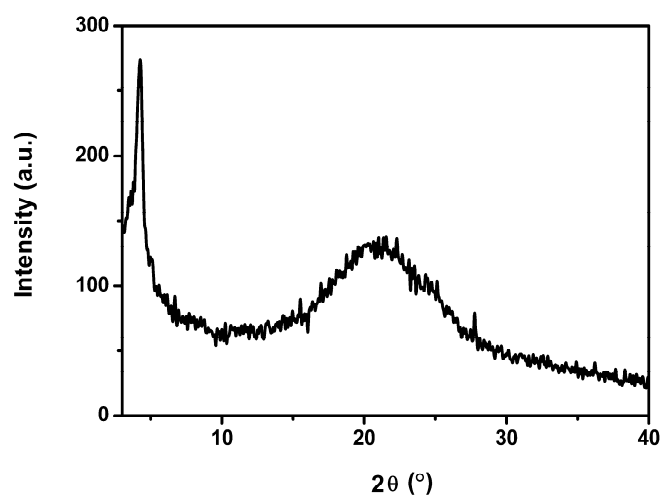


**Figure 3.** X-ray diffraction (XRD) pattern of PSTDPP film.

### 3.3. Hole Mobility

The incorporation of silolethiophene and benzodithiophene donor units and strong electron-drawing benzothiadiazole and diketopyrrolopyrrole units into the polymer backbones was expected to enhance hole transport mobility of the polymers. The organic field-effect transistors (OFETs) with a conventional bottom-contact and bottom-gate configuration were fabricated using the polymer as the active layer. Figure 4 shows the representative transfer and output current–voltage plots for the OFETs fabricated on an OTS treated Si/SiO<sub>2</sub> substrates. The devices showed a typical *p*-type transporting characteristic measured under ambient conditions. The PSTDPP based OFET exhibited relatively high hole mobility of  $2.2 \times 10^{-3} \text{ cm}^2 \cdot \text{V}^{-1} \cdot \text{s}^{-1}$  with an on/off ratio of  $10^6$ . The high mobility of the PSTDPP could be ascribed to the better molecular organization in the film. Furthermore, devices exhibited relatively high stability at ambient conditions. The devices were measured sequentially for about one month, and showed no obvious decline in the performance. The relatively high hole mobility is necessary for efficient charge transport in PSCs, which would be helpful to increase current density ( $J_{sc}$ ) and fill factors ( $FF$ ) of the devices [37].

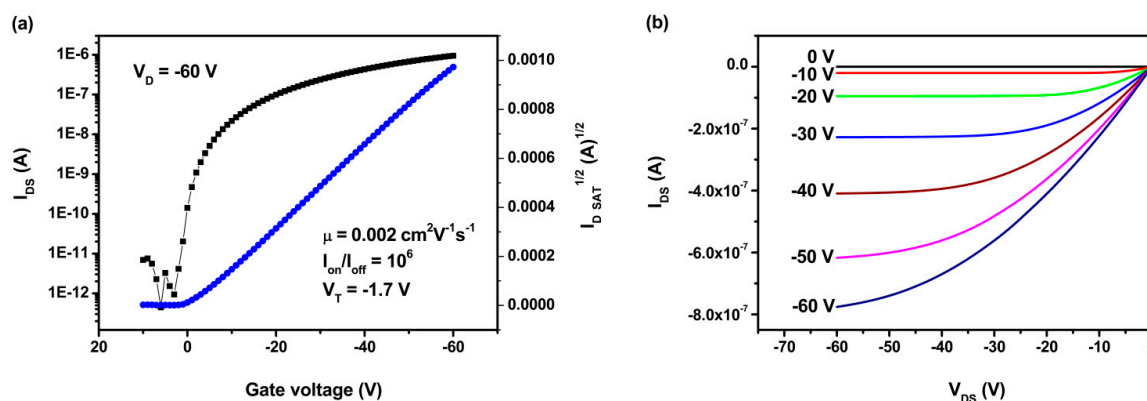


Figure 4. Transfer (a) and output (b) characteristics of PSTDPP.

### 3.4. Photovoltaic Properties

Since the polymer possessed proper energy levels and a suitable high mobility, it could be expected to show excellent photovoltaic performance. PSCs were fabricated with a conventional sandwich structure of ITO/PEDOT:PSS/polymer:PC<sub>71</sub>BM/Ca/Al, where the active layer was composed of PSTDPP as the donor and PC<sub>71</sub>BM as the acceptor. Different D/A ratios ( $w/w$ ) and processing solvents were systematically investigated to obtain the optimal device performance.

The device performances were firstly optimized by changing the D/A ratios of the polymer:PC<sub>71</sub>BM in ODCB solutions, and the optimal D/A ratio is 1:3 (Table 1). Then, further optimization was carried out by changing the processing solvents (from ODCB to CF or ODCB/CF blend). It was found that using CF as processing solvent was beneficial to the improvement of the open circuit voltage ( $V_{oc}$ ) and  $FF$ . Consequently, the solvent mixtures of ODCB and CF were chosen as processing solvents to investigate whether binary solvent can enhance the overall device performances. When using ODCB/CF (2/1,  $v/v$ ) as processing solvent, a much better PCE of 3.79% was obtained with  $J_{sc}$  of  $11.13 \text{ mA} \cdot \text{cm}^{-2}$ ,  $V_{oc}$  of 0.69 V and  $FF$  of 49.2%. At this point, all three parameters have been improved significantly compared with using ODCB as processing solvent. Finally, 1,8-diiodooctane (DIO) was added to the blend solution which was expected to tune the film morphology and device performance [38]. The resulting PCE for PSTDPP has grown to 4.38% by adding 2.5% DIO with further improvement of  $J_{sc}/FF$  and minor loss of  $V_{oc}$ .

The corresponding  $V_{oc}$ ,  $J_{sc}$ ,  $FF$  and PCE values of the devices are summarized in Table 1. Figure 5a shows the typical current density–voltage ( $J$ – $V$ ) curve of the PSC device fabricated the optimal condition by using the ternary solvents. The accuracy of the photovoltaic measurements for the

optimal device can be further confirmed by the EQE of the devices as showed in Figure 5b. The EQE curve exhibited a broader photoresponse in the range of 390 to 750 nm with EQE values of 42%–50%. The  $J_{sc}$  calculated from integration of the EQE curve was  $11.28 \text{ mA} \cdot \text{cm}^{-2}$ , which shows around 2.4% mismatch compared with the  $J_{sc}$  value obtained from the  $J$ - $V$  measurement.

**Table 1.** Photovoltaic properties of the PSTDPP/PC<sub>71</sub>BM-based bulk heterojunction (BHJ) solar cells fabricated with different solvents.

Solvent	D/A ( <i>w/w</i> )	$V_{oc}$ (V)	$J_{sc}$ ( $\text{mA cm}^{-2}$ )	FF (%)	PCE (%)
ODCB	1:1	0.51	5.53	34.8	0.98
ODCB	1:2	0.64	6.75	47.1	2.04
ODCB	1:3	0.63	9.89	37.9	2.35
ODCB	1:4	0.64	8.74	40.9	2.27
CF	1:3	0.69	1.68	50.9	0.59
ODCB:CF (2:1)	1:3	0.69	11.13	49.2	3.79
ODCB:CF (2:1) with 2.5%DIO	1:3	0.68	11.55	55.7	4.38

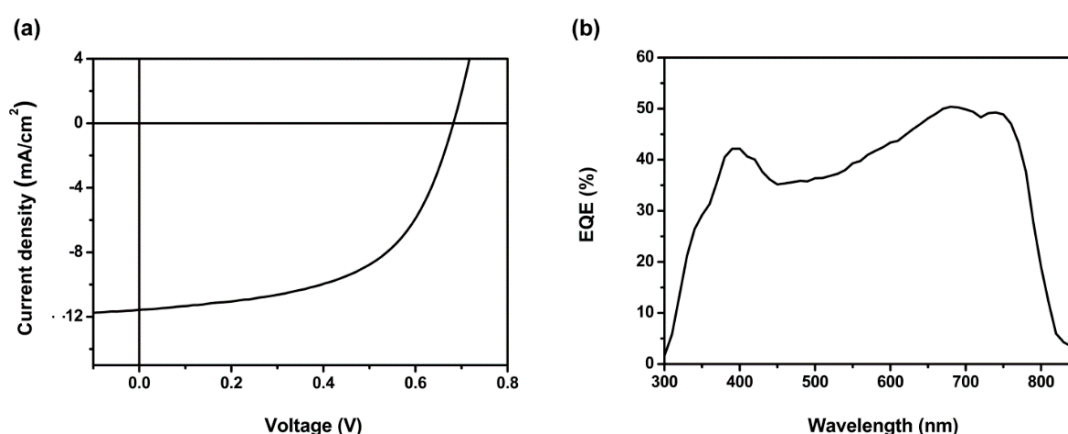


**Figure 5.** (a)  $J$ - $V$  curve of PSTDPP based BHJ solar cells prepared under the optimal condition (D/A ratio = 1:3, using *O*-dichlorobenzene (ODCB) and chloroform (CF) ( $v/v = 2:1$ ) with 2.5% DIO as processing solvent); and (b) EQE curve of the corresponding device.

### 3.5. Water Contact Angle Characterizations

Water contact angle characterizations were used to gain a deep insight of the surface components of the blend films processed by different solutions. As the decrease of water contact angle, the surface energy will increase and thus the top surface of the film will be more hydrophilic. Generally, water contact angle of polymer is bigger than that of PC<sub>71</sub>BM. For a blend film of BHJ solar cell composed by polymer and PC<sub>71</sub>BM, therefore, a smaller water contact angle indicates that PC<sub>71</sub>BM will be relatively enriched in the top surface of the blend film, and hence favorable ohmic contact with cathode will be formed, thus enhancing the photovoltaic performance of the corresponding device [19]. In fact, water contact angle of the blend film was affected, not only by the characters of polymer and PC<sub>71</sub>BM, but also by the preparation conditions of active layer. Figure 6 shows the respective water contact angles of four active-layer films prepared by different solvents. As shown, the water contact angle of the blend film prepared by CF is  $99.4^\circ \pm 0.3^\circ$ , which is far less than that of the blend film prepared by ODCB ( $105.1^\circ \pm 0.3^\circ$ ). Using the mixed solvent of ODCB/CF (2/1,  $v/v$ ) to prepare the blend film could decrease the water contact angle and the corresponding value is  $103.3^\circ \pm 0.5^\circ$ . Interestingly, when adding some amount of DIO to the mixed solvent, a smaller water contact angle of  $100.1^\circ \pm 0.4^\circ$  was observed similar to the blend film prepared by CF, indicating that PC<sub>71</sub>BM was relatively enriched in the top surface of the blend film in both cases and the corresponding BHJ solar cells might represent

relatively high photovoltaic performances accordingly [39,40]. Admittedly, this is just a possibility because the performance of PSC has a lot to do with the morphology of the active layer. Therefore, the analysis of morphology will be discussed in the following section.

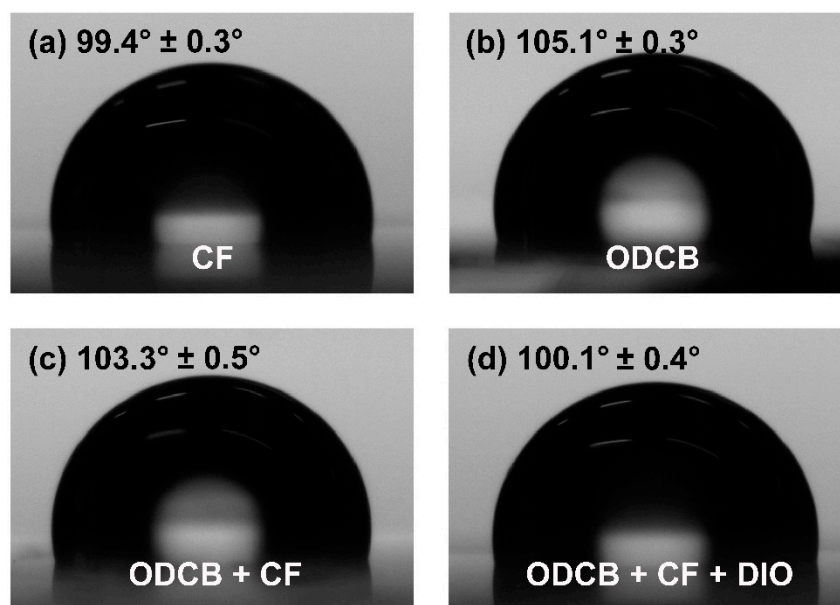


**Figure 6.** Water contact angle images of the top surface of (a) active-layer film prepared by CF; (b) active-layer film prepared by ODCB; (c) active-layer film prepared by ODCB:CF (2:1); and (d) active-layer film prepared by ODCB:CF (2:1) with 2.5% DIO.

### 3.6. Film Morphologies

Atomic force microscopy (AFM) was used to characterize the morphology of the active layers spin-coated from different solutions. AFM phase image of the blend film prepared by CF (Figure 7a) reveals a high level of aggregation in the active layer and the surface roughness of the film is 0.819 nm. The very clear large domains with sizes of hundreds of nanometers would diminish exciton migration to the D–A interface and influence the following charge separation and collection [41], leading to the worst performance for PSTDPP based PSCs. Using ODCB as the preparation solvent, the morphology of active layer has improved somewhat and the surface roughness becomes a little smoother (root mean square (RMS) roughness = 0.768 nm), but there are still some unequally distributed granular aggregations on the surface of the blend film (Figure 7b). Consequently, the overall performance of the corresponding device showed only moderate improvement. When introducing the mix solvent of ODCB and CF to the active layer preparation, an obvious change of film morphology was seen in the Figure 7c. The granular aggregations have disappeared from the phase image and the domain size has reduced to tens of nanometers. Although the roughness of the film is 0.803 nm, the film morphology is much better than that of the above two cases, so the PCE exhibited a significant improvement. Finally, the optimized morphology was obtained by adding additive (DIO) to the mixed solvent. The roughness of the film has drop to 0.751 nm and the surface of the blend film becomes much smoother (Figure 7d), which is beneficial to the higher efficiency of exciton diffusion as well as charge separation [42]. In addition, combined with the water contact angle result, the best photovoltaic performance was eventually achieved for PSTDPP based PSCs with a ternary solvent.

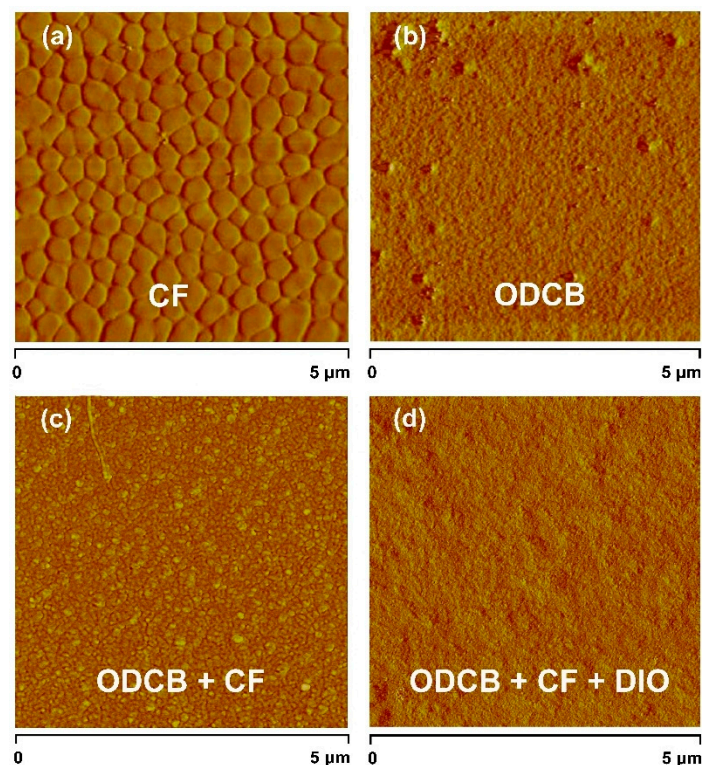


**Figure 7.** AFM phase image of PSTDPP/PC<sub>71</sub>BM blend film prepared by different solvents. (a) CF; (b) ODCB; (c) ODCB:CF (2:1); and (d) ODCB:CF (2:1) with 2.5% DIO. The size of the AFM image is 5 μm × 5 μm.

#### 4. Conclusions

In summary, a new random copolymer containing two donors (SDT and BDT) and two acceptors (BT and DPP), named as PSTDPP, has been synthesized and fully characterized. As expected, the random polymer exhibits a broad absorption with a range of 500–800 nm and a proper HOMO energy level, which ensure its applicability for fabrication of PSC devices. When using ODCB as processing solvent, a moderate PCE of 2.35% was obtained. To further optimize the device performances of PSTDPP/PC<sub>71</sub>BM-based PSCs, different processing solvents (from ODCB to CF or ODCB/CF blend) were systematically investigated. It was found that the solvent mixtures of ODCB and CF with small amount of DIO as additive could offer a much better active layer with PC<sub>71</sub>BM enriched surface composition and improved morphology, which led to a significantly enhanced PCE of 4.38% compared with using ODCB as processing solvent. These results indicate that constructing random copolymer with multiple donor and acceptor monomers could provide a new general method for designing photovoltaic polymers with optimized optical and electrochemical properties. In addition, introducing proper mixed solvents to the active layer preparation is a very promising approach to improve the characteristics of the film, which would be very conducive to achieving high PSC performance.

**Acknowledgments:** We acknowledge the financial support of the National Natural Science Foundation of China (Grant Nos. 21125420, 21474022 and 21101010) and the Ministry of Science and Technology of China (No. 2013CB834700).

**Author Contributions:** Kun Lu, Tianyi Zhao, Zhixiang Wei and Lei Jiang designed the experiments. Xiangwei Zhu, Benzhen Xia, Jin Fang and Yifan Zhao carried out the initial experiments. Xiangwei Zhu and Kun Lu carried out further experiments and wrote the manuscript. All authors discussed the data and commented on the manuscript.

**Conflicts of Interest:** The authors declare no conflict of interest.

## References

1. Yu, G.; Gao, J.; Hummelen, J.C.; Wudl, F.; Heeger, A.J. Polymer photovoltaic cells: Enhanced efficiencies via a network of internal donor-acceptor heterojunctions. *Science* **1995**, *270*, 1789–1791. [[CrossRef](#)]
2. Chen, J.; Cao, Y. Development of novel conjugated donor polymers for high-efficiency bulk-heterojunction photovoltaic devices. *Acc. Chem. Res.* **2009**, *42*, 1709–1718. [[CrossRef](#)] [[PubMed](#)]
3. Inganäs, O.; Zhang, F.; Andersson, M.R. Alternating polyfluorenes collect solar light in polymer photovoltaics. *Acc. Chem. Res.* **2009**, *42*, 1731–1739. [[CrossRef](#)] [[PubMed](#)]
4. Li, Y. Molecular design of photovoltaic materials for polymer solar cells: Toward suitable electronic energy levels and broad absorption. *Acc. Chem. Res.* **2012**, *45*, 723–733. [[CrossRef](#)] [[PubMed](#)]
5. He, Z.; Xiao, B.; Liu, F.; Wu, H.; Yang, Y.; Xiao, S.; Wang, C.; Russell, T.P.; Cao, Y. Single-junction polymer solar cells with high efficiency and photovoltage. *Nat. Photonics* **2015**, *9*, 174–179. [[CrossRef](#)]
6. Vohra, V.; Kawashima, K.; Kakara, T.; Koganezawa, T.; Osaka, I.; Takimiya, K.; Murata, H. Efficient inverted polymer solar cells employing favourable molecular orientation. *Nat. Photonics* **2015**, *9*, 403–408. [[CrossRef](#)]
7. Dou, L.; Chen, C.-C.; Yoshimura, K.; Ohya, K.; Chang, W.-H.; Gao, J.; Liu, Y.; Richard, E.; Yang, Y. Synthesis of 5h-dithieno[3,2-b:2',3'-d]pyran as an electron-rich building block for donor-acceptor type low-bandgap polymers. *Macromolecules* **2013**, *46*, 3384–3390. [[CrossRef](#)]
8. Kroon, R.; Diaz de Zerio Mendaza, A.; Himmelberger, S.; Bergqvist, J.; Bäcke, O.; Faria, G.C.; Gao, F.; Obaid, A.; Zhuang, W.; Gedefaw, D.; *et al.* A new tetracyclic lactam building block for thick, broad-bandgap photovoltaics. *J. Am. Chem. Soc.* **2014**, *136*, 11578–11581. [[CrossRef](#)] [[PubMed](#)]
9. Huang, Y.; Liu, F.; Guo, X.; Zhang, W.; Gu, Y.; Zhang, J.; Han, C.C.; Russell, T.P.; Hou, J. Manipulating backbone structure to enhance low band gap polymer photovoltaic performance. *Adv. Energy Mater.* **2013**, *3*, 930–937. [[CrossRef](#)]
10. Mei, J.; Bao, Z. Side chain engineering in solution-processable conjugated polymers. *Chem. Mater.* **2014**, *26*, 604–615. [[CrossRef](#)]
11. Price, S.C.; Stuart, A.C.; Yang, L.; Zhou, H.; You, W. Fluorine substituted conjugated polymer of medium band gap yields 7% efficiency in polymer–fullerene solar cells. *J. Am. Chem. Soc.* **2011**, *133*, 4625–4631. [[CrossRef](#)] [[PubMed](#)]
12. Kang, T.E.; Kim, K.-H.; Kim, B.J. Design of terpolymers as electron donors for highly efficient polymer solar cells. *J. Mater. Chem. A* **2014**, *2*, 15252–15267. [[CrossRef](#)]
13. Nielsen, C.B.; Ashraf, R.S.; Schroeder, B.C.; D'Angelo, P.; Watkins, S.E.; Song, K.; Anthopoulos, T.D.; McCulloch, I. Random benzotrithiophene-based donor-acceptor copolymers for efficient organic photovoltaic devices. *Chem. Commun.* **2012**, *48*, 5832–5834. [[CrossRef](#)] [[PubMed](#)]
14. Jung, J.W.; Liu, F.; Russell, T.P.; Jo, W.H. Semi-crystalline random conjugated copolymers with panchromatic absorption for highly efficient polymer solar cells. *Energ. Environ. Sci.* **2013**, *6*, 3301–3307. [[CrossRef](#)]
15. Kang, T.E.; Cho, H.-H.; Kim, H.j.; Lee, W.; Kang, H.; Kim, B.J. Importance of optimal composition in random terpolymer-based polymer solar cells. *Macromolecules* **2013**, *46*, 6806–6813. [[CrossRef](#)]
16. Wang, L.; Shi, S.; Ma, D.; Chen, S.; Gao, C.; Wang, M.; Shi, K.; Li, Y.; Li, X.; Wang, H. Improved photovoltaic properties of donor-acceptor copolymers by introducing quinoxalino[2,3-b']porphyrin as a light-harvesting unit. *Macromolecules* **2015**, *48*, 287–296. [[CrossRef](#)]
17. Cho, N.; Yip, H.-L.; Jen, A.K.-Y. Morphology evolution by controlling solvent-solute interactions using a binary solvent in bulk heterojunction solar cells. *Appl. Phys. Lett.* **2013**, *102*, 233903. [[CrossRef](#)]
18. Ye, L.; Zhang, S.; Ma, W.; Fan, B.; Guo, X.; Huang, Y.; Ade, H.; Hou, J. From binary to ternary solvent: Morphology fine-tuning of D/A blends in PDPP3T-based polymer solar cells. *Adv. Mater.* **2012**, *24*, 6335–6341. [[CrossRef](#)] [[PubMed](#)]
19. Ye, L.; Jing, Y.; Guo, X.; Sun, H.; Zhang, S.; Zhang, M.; Huo, L.; Hou, J. Remove the residual additives toward enhanced efficiency with higher reproducibility in polymer solar cells. *J. Phys. Chem. C* **2013**, *117*, 14920–14928. [[CrossRef](#)]
20. Son, S.K.; Lee, H.-S.; Ha, J.S.; Kim, K.H.; Son, H.J.; Ko, M.J.; Kim, H.; Lee, D.-K.; Kim, J.Y.; Lee, W.; *et al.* Effect of asymmetric solubility of diketopyrrolopyrrole-based polymers and PC71BMS in a binary solvent system on the performance of bulk heterojunction solar cells. *Solar Energy Mater. Solar Cells* **2014**, *124*, 232–240. [[CrossRef](#)]

21. Wang, D.; Zhang, F.; Li, L.; Yu, J.; Wang, J.; An, Q.; Tang, W. Tuning nanoscale morphology using mixed solvents and solvent vapor treatment for high performance polymer solar cells. *RSC Adv.* **2014**, *4*, 48724–48733. [[CrossRef](#)]
22. Van Franeker, J.J.; Turbiez, M.; Li, W.; Wienk, M.M.; Janssen, R.A.J. A real-time study of the benefits of co-solvents in polymer solar cell processing. *Nat. Commun.* **2015**, *6*. [[CrossRef](#)] [[PubMed](#)]
23. Hou, J.; Chen, H.-Y.; Zhang, S.; Li, G.; Yang, Y. Synthesis, characterization, and photovoltaic properties of a low band gap polymer based on silole-containing polythiophenes and 2,1,3-benzothiadiazole. *J. Am. Chem. Soc.* **2008**, *130*, 16144–16145. [[CrossRef](#)] [[PubMed](#)]
24. Hou, J.H.; Park, M.H.; Zhang, S.Q.; Yao, Y.; Chen, L.M.; Li, J.H.; Yang, Y. Bandgap and molecular energy level control of conjugated polymer photovoltaic materials based on benzo[1,2-*b*:4,5-*b'*]dithiophene. *Macromolecules* **2008**, *41*, 6012–6018. [[CrossRef](#)]
25. Dhanabalan, A.; van Duren, J.K.J.; van Hal, P.A.; van Dongen, J.L.J.; Janssen, R.A.J. Synthesis and characterization of a low bandgap conjugated polymer for bulk heterojunction photovoltaic cells. *Adv. Funct. Mater.* **2001**, *11*, 255–262. [[CrossRef](#)]
26. Wienk, M.M.; Turbiez, M.; Gilot, J.; Janssen, R.A.J. Narrow-bandgap diketo-pyrrolo-pyrrole polymer solar cells: The effect of processing on the performance. *Adv. Mater.* **2008**, *20*, 2556–2560. [[CrossRef](#)]
27. Gupta, V.; Kyaw, A.K.K.; Wang, D.H.; Chand, S.; Bazan, G.C.; Heeger, A.J. Barium: An efficient cathode layer for bulk-heterojunction solar cells. *Sci. Rep.* **2013**, *3*, 1965. [[CrossRef](#)] [[PubMed](#)]
28. Ye, L.; Zhang, S.; Zhao, W.; Yao, H.; Hou, J. Highly efficient 2D-conjugated benzodithiophene-based photovoltaic polymer with linear alkylthio side chain. *Chem. Mater.* **2014**, *26*, 3603–3605. [[CrossRef](#)]
29. Liu, Y.; Zhao, J.; Li, Z.; Mu, C.; Ma, W.; Hu, H.; Jiang, K.; Lin, H.; Ade, H.; Yan, H. Aggregation and morphology control enables multiple cases of high-efficiency polymer solar cells. *Nat. Commun.* **2014**, *5*, 5293. [[CrossRef](#)] [[PubMed](#)]
30. Choi, H.; Ko, S.-J.; Kim, T.; Morin, P.-O.; Walker, B.; Lee, B.H.; Leclerc, M.; Kim, J.Y.; Heeger, A.J. Small-bandgap polymer solar cells with unprecedented short-circuit current density and high fill factor. *Adv. Mater.* **2015**, *27*, 3318–3324. [[CrossRef](#)] [[PubMed](#)]
31. Huo, L.; Hou, J.; Chen, H.-Y.; Zhang, S.; Jiang, Y.; Chen, T.L.; Yang, Y. Bandgap and molecular level control of the low-bandgap polymers based on 3,6-dithiophen-2-yl-2,5-dihydropyrrolo[3,4-*c*]pyrrole-1,4-dione toward highly efficient polymer solar cells. *Macromolecules* **2009**, *42*, 6564–6571. [[CrossRef](#)]
32. Liang, Y.; Wu, Y.; Feng, D.; Tsai, S.-T.; Son, H.-J.; Li, G.; Yu, L. Development of new semiconducting polymers for high performance solar cells. *J. Am. Chem. Soc.* **2009**, *131*, 56–57. [[CrossRef](#)] [[PubMed](#)]
33. Bürgi, L.; Turbiez, M.; Pfeiffer, R.; Bienewald, F.; Kirner, H.-J.; Winnewisser, C. High-mobility ambipolar near-infrared light-emitting polymer field-effect transistors. *Adv. Mater.* **2008**, *20*, 2217–2224. [[CrossRef](#)]
34. Takacs, C.J.; Sun, Y.; Welch, G.C.; Perez, L.A.; Liu, X.; Wen, W.; Bazan, G.C.; Heeger, A.J. Solar cell efficiency, self-assembly, and dipole–dipole interactions of isomorphous narrow-band-gap molecules. *J. Am. Chem. Soc.* **2012**, *134*, 16597–16606. [[CrossRef](#)] [[PubMed](#)]
35. Sun, Q.; Wang, H.; Yang, C.; Li, Y. Synthesis and electroluminescence of novel copolymers containing crown ether spacers. *J. Mater. Chem.* **2003**, *13*, 800–806. [[CrossRef](#)]
36. Lu, K.; Fang, J.; Yu, Z.; Yan, H.; Zhu, X.; Zhang, Y.; He, C.; Wei, Z. Improving the performance of polymer solar cells by altering polymer side chains and optimizing film morphologies. *Organic Electronics* **2012**, *13*, 3234–3243. [[CrossRef](#)]
37. He, Y.; Wu, W.; Zhao, G.; Liu, Y.; Li, Y. Poly(3,6-dihexyl-thieno[3,2-*b*]thiophene vinylene): Synthesis, field-effect transistors, and photovoltaic properties. *Macromolecules* **2008**, *41*, 9760–9766. [[CrossRef](#)]
38. Lee, J.K.; Ma, W.L.; Brabec, C.J.; Yuen, J.; Moon, J.S.; Kim, J.Y.; Lee, K.; Bazan, G.C.; Heeger, A.J. Processing additives for improved efficiency from bulk heterojunction solar cells. *J. Am. Chem. Soc.* **2008**, *130*, 3619–3623. [[CrossRef](#)] [[PubMed](#)]
39. Kiel, J.W.; Kirby, B.J.; Majkrzak, C.F.; Maranville, B.B.; Mackay, M.E. Nanoparticle concentration profile in polymer-based solar cells. *Soft Matter* **2010**, *6*, 641–646. [[CrossRef](#)]
40. Staniec, P.A.; Parnell, A.J.; Dunbar, A.D.F.; Yi, H.; Pearson, A.J.; Wang, T.; Hopkinson, P.E.; Kinane, C.; Dalgliesh, R.M.; Donald, A.M.; *et al.* The nanoscale morphology of a PCDTBT:PCBM photovoltaic blend. *Adv. Energy Mater.* **2011**, *1*, 499–504. [[CrossRef](#)]

41. Chung, H.-S.; Lee, W.-H.; Song, C.E.; Shin, Y.; Kim, J.; Lee, S.K.; Shin, W.S.; Moon, S.-J.; Kang, I.-N. Highly conjugated side-chain-substituted benzo[1,2-b:4,5-b']dithiophene-based conjugated polymers for use in polymer solar cells. *Macromolecules* **2013**, *47*, 97–105. [[CrossRef](#)]
42. Guo, X.; Cui, C.H.; Zhang, M.J.; Huo, L.J.; Huang, Y.; Hou, J.H.; Li, Y. High efficiency polymer solar cells based on poly(3-hexylthiophene)/indene-C<sub>70</sub> bisadduct with solvent additive. *Energ. Environ Sci.* **2012**, *5*, 7943–7949. [[CrossRef](#)]



© 2015 by the authors; licensee MDPI, Basel, Switzerland. This article is an open access article distributed under the terms and conditions of the Creative Commons by Attribution (CC-BY) license (<http://creativecommons.org/licenses/by/4.0/>).